1. Introduction

Ridges in tilled fields are a common feature of the microrelief at the earth's surface in most agricultural areas of the world, and they are often used as part of wind erosion control systems. When the vegetation is removed for food, fuel, or fodder, ridges and soil aggregation are frequently the only means of wind erosion control on large areas. Thus, understanding the factors that control soil loss by wind erosion from ridged fields is important in designing adequate wind erosion systems.

In section 2, we will briefly review the literature on ridges and describe the field surface factors that control soil loss from nonvegetated ridged fields. In section 3, a wind tunnel experiment to determine one of the control factors, ridge trapping efficiency, is described, and some results of the experiment are discussed in section 4. Finally, a simple example of field soil loss as affected by trapping efficiency is presented in section 5.

2. Soil surface control factors

Wind erosion on a ridged field surface is complex and there are at least four major simultaneous processes affecting soil loss (figure 1). First, there is removal of loose, erodible-size (< 0.84 mm diameter) particles from among the large clods by wind. This soil loss, E, is mostly removed from the upwind slope and top of the ridge. (All symbols are defined in table 1.) Loose soil loss has been measured for many unridged surfaces in wind tunnels and Fryrear (1984) showed that for a variety of surface covers, E was approximately

$$E = m - n \ln(SC), \quad (SC) > 10 \qquad [1]$$

where m and n are coefficients that likely vary with windspeed and SC is percent soil cover of flat residues or clods.

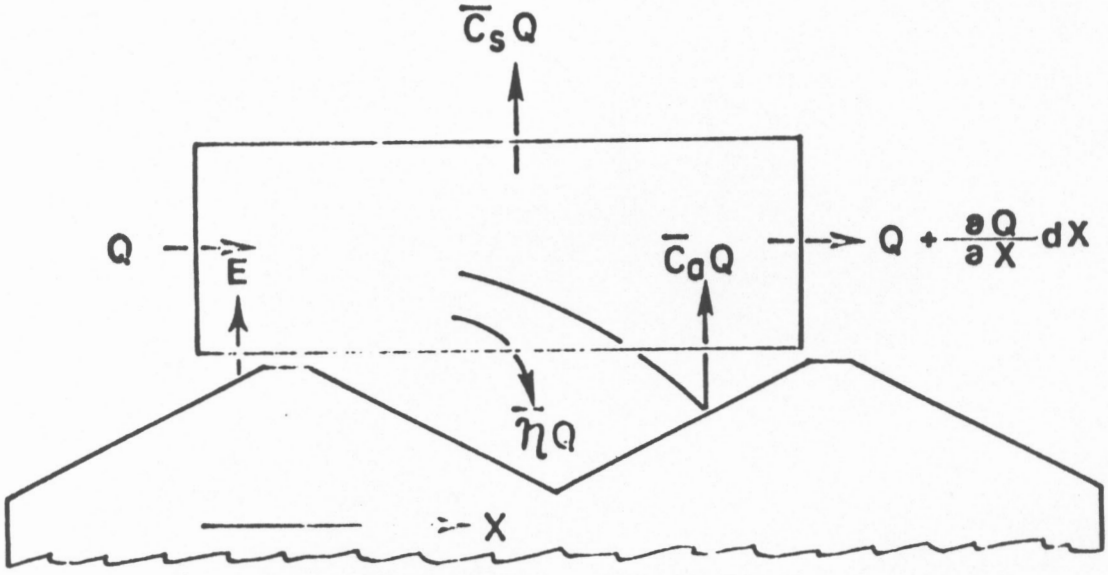

Figure 1 Ridge schematic and control surface for mass balance in the saltation region.

Table 1. Notation. M, L, and T as dimensions refer to mass, length, and time.

Symbol	Definition and Dimensions
A	Ridge height, L
A_0	Initial ridge height, L
a	Ridge height reduction by erosion, L
C	Percent soil cloddiness (≥ 0.84 mm diameter) by weight
$\bar{C}_a$	Average abrasion coefficient, L^{-1}
$\bar{C}_s$	Average suspension coefficient, L^{-1}
C_1	Constant
C_4	Constant, L^{-2}
d	Constant
d_p	Particle diameter, L
e	Constant
E	Loose surface soil removable by wind, ML^{-2}
g	Constant
h	Interridge height filled with loose soil, L
L	Length of tunnel covered by ridges in X - direction, L
m, n	Coefficients, ML^{-2}
Q	Total horizontal soil passage per unit width, ML^{-1}
q	Horizontal soil flux integrated over the saltation height per unit width, $ML^{-1}T^{-1}$
Sa	Soil aggregate mechanical stability, MT^{-2}
SC	Percent soil cover of flat residues or clods
T	Total time, T
t	Time, T
U_∞	Wind tunnel freestream windspeed, LT^{-1}

U_*	Friction velocity, LT^{-1}
V_1	Ridge top loss volume from erosion per unit horizontal area before ridge height is reduced, L
V_2	Additional ridge top loss volume from erosion per unit horizontal area when ridge height is reduced, L
V_3	Interridge volume filled by loose soil per unit horizontal area, L
V_p	Particle impact velocity, LT^{-1}
w	Soil clod abrasive wear
x	Downwind distance, L
α	Saltating particle impact angle, degrees
λ	Ridge wavelength, L
η	Fraction of passing q trapped by ridges and herein called ridge trapping efficiency, L^{-1}
$\bar{\eta}$	Average fraction of passing Q trapped by ridges, L^{-1}
η_0	Initial ridge trapping efficiency, L^{-1}
ρ_b	Soil bulk density, ML^{-3}

Armbrust, Chepil, and Siddoway (1964) measured E from a 1.62 m long tray using 1 to 20 cm - tall ridges in a wind tunnel and showed that E could be reduced as much as 50 percent on ridged surfaces compared to unridged surfaces with the same soil cloddiness and friction velocity (U_*). Nevertheless, the slope n of their soil loss curves was similar to Fryrear's, and E averaged over U_* of 0.9 to 1.08 m/s was

$$E = 8.12 + 0.045\ A_e - 2.28\ \ln(C),\ (C) > 10,\ A_e > 2.5 \qquad [2]$$

where E is Kg/m^2, A_e is ridge height in cm, and C is percent soil cloddiness (> 0.84 mm diameter) by weight.

Removal of the loose soil usually allows the upwind field surface to stabilize. Unfortunately, the downwind surface clods and crust are abraded by the saltating loose soil from upwind. The abrasion creates additional saltation and suspension-size particles and also exposes additional erodible particles as the surface is abraded away. There appear to be no direct measurements of abrasion on ridges, but it is probable that the process is not greatly different than on an unridged surface, except that on ridges, the abrasion zone is concentrated along the upper 2/3 of the upwind ridge face. For unridged surfaces composed of mixtures of clods and saltation-size particles, Hagen[1] found on wind tunnel trays that soil loss from abrasion varied linearly with the total saltation passage (Q) and the abrasion coefficient (C_a) varied with C. Thus, for a ridged surface, a first approximation is that abrasion loss equals $\bar{C}_a Q$ where $\bar{C}_a$ is an average abrasion coefficient for the surface layer.

1] Unpublished data of Hagen.

$\bar{C}_a$ also varies inversely with the mechanical stability of the clods and crust. Chepil and Woodruff (1963) discussed the formation of various soil structural units and listed their relative mechanical stability in the dry state from highest to lowest as follows: (a) water-stable aggregates, (b) secondary aggregates or clods, (c) surface crust, and (d) fine materials among the clods. Hagen (1984) abraded individual soil clods with a sand blasting nozzle and found that abrasive erosion of the clods was inversely related to clod mechanical stability as measured by a drop-shatter test (figure 2). Above a threshold particle impact velocity, abrasive erosion from the target aggregates also was proportional to particle impact kinetic energy.

Another process illustrated in figure 1 is the removal of the finest fraction of moving soil from the top of the saltation region. This suspension is postulated as the product of Q and an average suspension coefficient $\bar{C}_s$. $\bar{C}_s$ likely varies along the wind direction and changes with windspeed, but in a manner presently unknown. Gillette (1977) measured a portion of the suspension flux (< 20 μm diameter) on several fields and found that it varied widely on different soil textures. Hagen and Lyles (1985) found that during initial impacts of saltation-size particles in an enclosed chamber, the major source of particles < 50 μm diameter was the impacting soil particles and not the target aggregate. Much additional work appears necessary to specify $\bar{C}_s$ on most soils.

A final process is the trapping of the saltation flux in the interridge areas, which can significantly reduce the total impact kinetic energy on the field surface. For example, trapping saltating particles within 5 to 10 m of their initial movement instead of allowing them to travel to a field border 100 m downwind would reduce impact kinetic energy on the surface 10 to 20

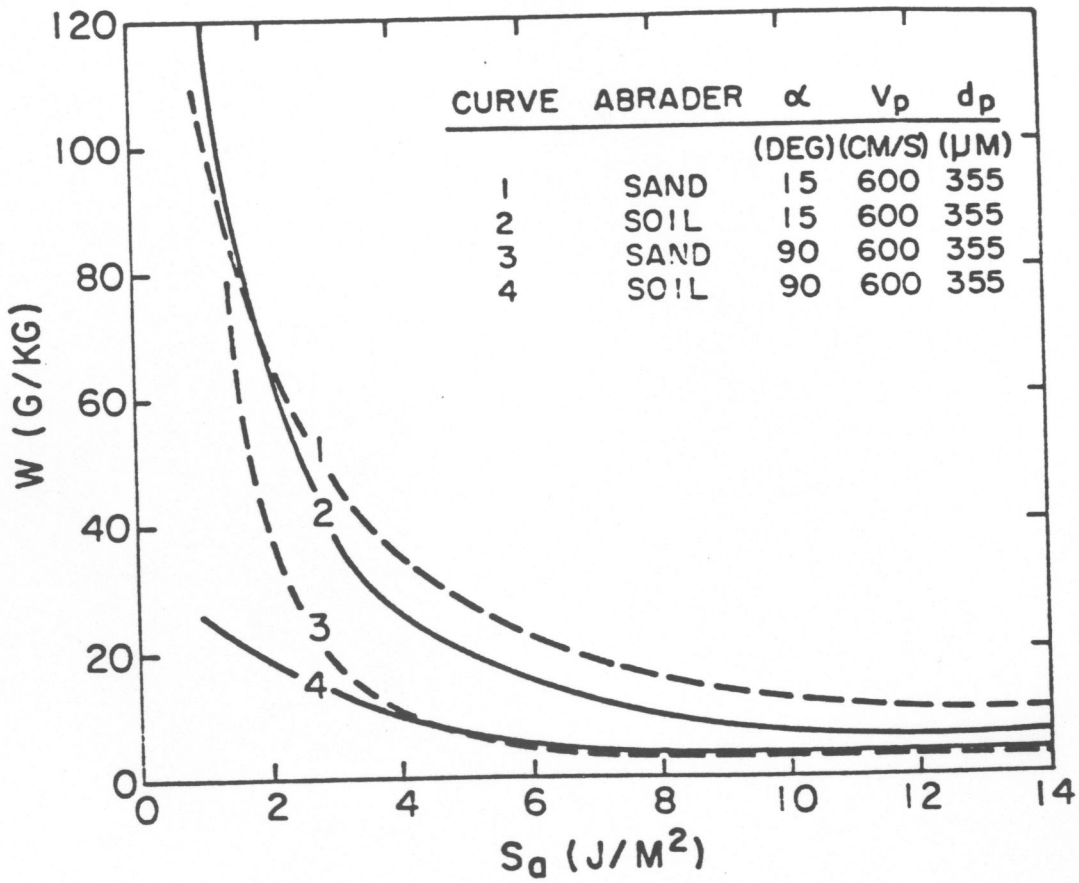

Figure 2 Predicted aggregate abrasive erosion (w) as a function of aggregate stability (Sa) for various impact angles (α), impact velocities (V_p) and particle diameters (d_p).

times. Thus, both the trapping efficiency (η) in dimensions [1/L] and the interridge volume available to maintain η are important. Because data on η are lacking, an experiment to measure η was undertaken.

3. *Experimental procedure for η*

Ridges composed of a mixture of 2 to 6 mm diameter gravel and 0.29 to 0.42 mm quartz sand were constructed normal to the flow along 610 cm of the working section of a wind tunnel which is 76 cm wide and 91 tall. For each set of test ridges, the tunnel roof was adjusted to give zero pressure gradient in the working section, and the loose soil on the ridge tops was removed by operating the tunnel until the ridges were armored on the upwind side. Thus, during the trapping experiments E, $\bar{C}_s$, and $\bar{C}_a$ were all equal to zero (figure 1).

Freestream velocity was measured above the ridges using a pitot-static tube. Next, a weighed amount of sand (0.29 to 0.42 mm diameter) was placed on the tunnel floor upwind of the ridges, and the tunnel operated for 3 to 5 minutes with a relatively constant sand flux entering the ridges. At the downwind side of the ridges, a vertical slot sampler collected the saltating sand in a pan mounted on a recording load cell below the tunnel floor. Finally, the remaining sand on the floor upwind was reweighed and the loss was compared to the flux that had passed the sampler. The difference was the sand trapped by the ridges.

To calculate η, the ridges were assumed to act like a series of filters, which, using the conservation of mass principle, can be modeled as

$$-\frac{dq}{dx} = \eta q \qquad [3]$$

and for short runs with q and η in steady state, integrating gives

$$\eta = \ln (Q_{in}/Q_{out})/L \qquad [4]$$

Figure 2 Predicted aggregate abrasive erosion (w) as a function of aggregate stability (Sa) for various impact angles (α), impact velocities (V_p) and particle diameters (d_p).

where q is the soil flux in the X-direction integrated over the saltation height, L is ridge-covered tunnel length (6.1 m), and Q is the time integral of q. Each set of ridges was tested at three freestream windspeeds (U_∞), ranging between 10 and 15.5 m/s. For the two largest windspeeds, a second flux rate was created at each windspeed by adding a low wire screen barrier in front of the upwind sand source.

Ridges that had substantial capacity were next filled with saltating sand at U_∞ of 10 m/s and then eroded by wind alone to static equilibrium (q = 0) at 15.5 m/s. These ridges were then subjected again to an upwind sand flux to determine at what windspeeds sand was deposited or entrained from between the ridges. In this way, an approximate dynamic equilibrium (η = 0) for ridges could be determined.

Surface contour of each set of ridges was measured over 1 or 2 wavelengths by lowering a laser beam until it was focused on the ridge surface and then observing the relative change in height from a scale fastened to the laser optics. The test ridges had height (A) to wave length (λ) ratios of 0.11, 0.15, 0.18, and 0.21; heights of 2.4, 4.5, 6.5, and 8.0 cm; and sand flux rates (q) of 0.1 to 0.6 g/cm·s.

4. Results and discussion for η

A total of 25 test runs of trapping efficiency were analyzed using a stepwise regression procedure, and the best 6- variable model found was

$$\eta = -0.0264 + 1.342\,(A/\lambda) - 0.67\,(q^2) - 15 \times 10^{-4}\,(U_\infty^2) + 0.05614\,(qU_\infty) + 0.04517\,(qA) - 2.09755\,(qA/\lambda) \qquad [5]$$

where the units are A and λ in cm, q in g/cm·s, and U_∞ in m/s. The coefficient of multiple determination (R^2) for the model was 0.82.

A plot of the model shows that η was strongly influenced by windspeed (figure 3). The ridge with A/λ equal 0.11 was statically stable with U_∞ equal 15.5 m/s, but dynamically stable ($\eta = 0$) at 10.3 m/s. Thus, the dynamic to static threshold windspeed ratio was about 0.66, which is less than the value of 0.8 usually cited for all-erodible surfaces (Bagnold, 1941). The decrease in the ratio probably occurs because saltating particles are more effective than wind alone in carrying momentum to the surface leeward of the ridges.

Vertical profiles of the saltation flux were markedly changed by the underlying surface and thus, also likely affected η. To compare profiles, a relative flux was calculated as the ratio of flux to maximum flux for each profile. The relative saltation flux increased near the surface of the ridge tops as ridge amplitude increased from an unridged surface to maximum amplitude (figures 4, 5, 6). In the case of the unridged surface (figure 4), the absolute flux gradient above 5 cm decreased as windspeed increased. Similarly, immediately above the ridges, increasing windspeed also decreased the absolute gradient of the horizontal flux, while gradients above 20 cm were less affected than those below. Evidently, trapping of particles from the lower portion of the flux profile reduces the absolute gradient above ridges. The low flux values in the lowest portion of the interridge area in figure 6 demonstrate that most of the flux impacted along the upper portion of the windward ridge face.

Finally, another plot of equation 5 shows that there was an asymptotic increase in η as the input flux was increased at a fixed windspeed (figure 7). It is probable that adding particles to the stream reduces the momentum absorbed by individual particles, so they move more slowly and are easier to

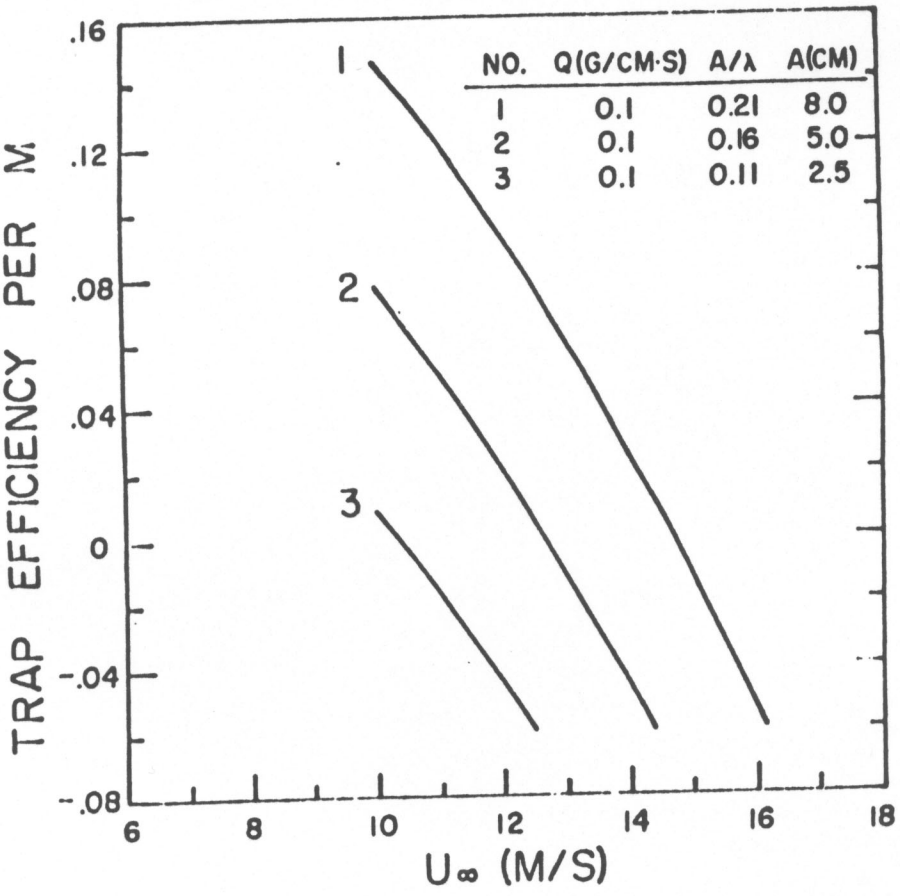

Figure 3 Values of η predicted by equation 5 as a function of freestream windspeed.

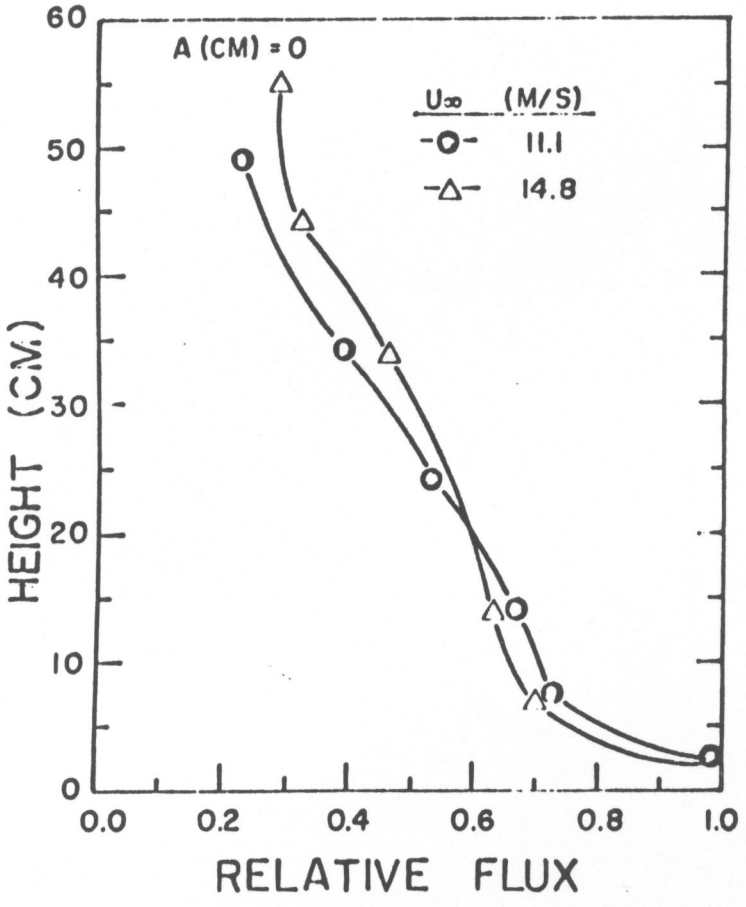

Figure 4 Relative sand flux distribution as affected by freestream windspeed for unridged surface.

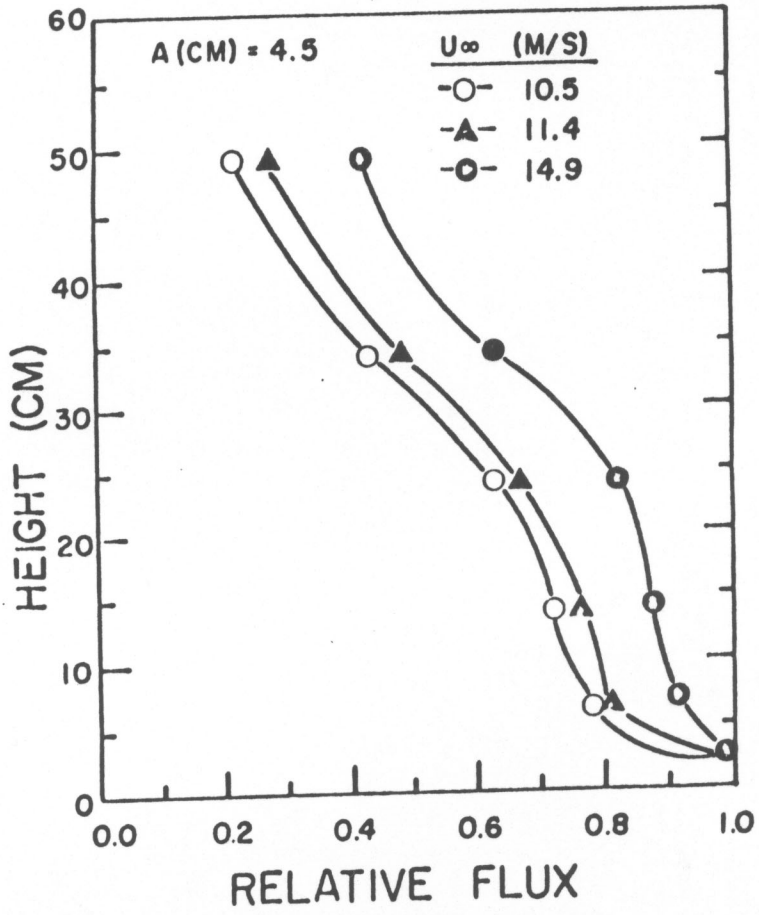

Figure 5 Relative sand flux distribution as affected by freestream windspeed for 4.5 cm tall ridges of wavelength 21.5 cm. (Height measured from lowest interridge surface.)

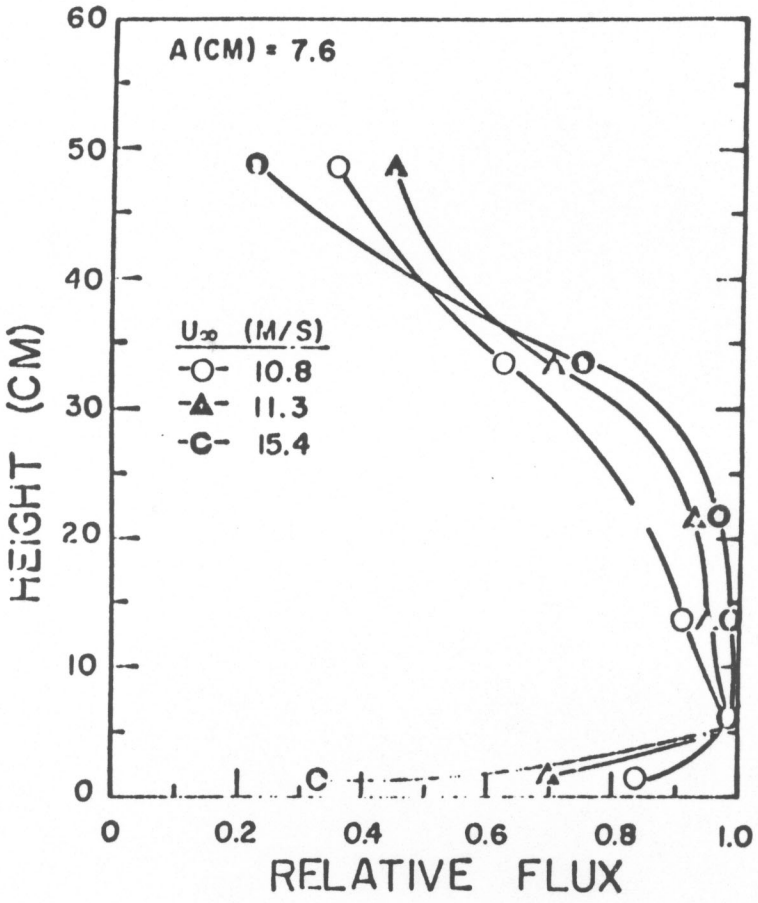

Figure 6 Relative sand flux distribution as affected by freestream windspeed for 7.6 cm tall ridges of wavelength 43 cm. (Height measured from lowest interridge surface.)

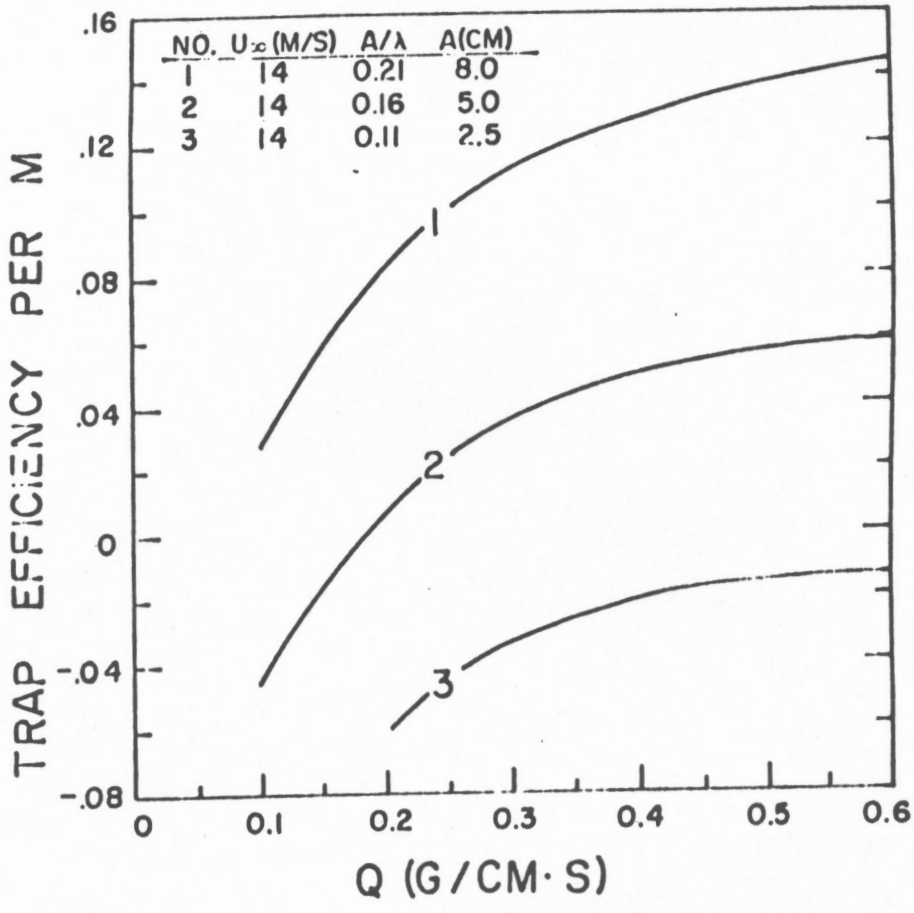

Figure 7 Values of n predicted by equation 5 as a function of saltation flux passing the ridges.

trap. Increasing both A and A/λ also tended to increase η. However, there is a practical limit of about 0.25 for A/λ for most soils, which is imposed by the angle of repose of the soil materials.

5. Simple field example

Cole (1984) has pointed out that for a general solution to field soil loss, one must integrate the governing flux equations in both time and space, because wind erosion is a time and space dependent process. However, in windy, semi-arid regions one wants the field surface to stabilize long before the winds cease. For such designs, total soil loss will not depend on total wind energy but, instead, each field will have a maximum soil loss governed by the field surface. For such a field, total horizontal soil passage (Q) at any downwind location (x) is

$$Q = \int_0^T q \, dt \qquad [6]$$

where q is horizontal soil flux and t is time. Here we will consider a simple example of such a field to illustrate the importance of η.

To further simplify the example, consider a region where the erosive wind direction is nearly constant and the ridges are oriented normal to the wind direction. Then, for conservation of mass along the wind direction from figure 1

$$\frac{dQ}{dx} = E - \bar{\eta} Q + \bar{C}_a Q - \bar{C}_s Q \qquad [7]$$

where E is loose soil removable from the ridge tops by wind alone [M/L^2],

$\bar{\eta}$ is average fraction of passing Q trapped by the ridges [1/L],

$\bar{C}_a$ is average additional soil abraded per unit passing Q [1/L], and

$\bar{C}_s$ is average soil suspended per unit passing Q [1/L].

While $\bar{C}_s$ can be significant on certain soils, for the present example we will assume $\bar{C}_s = 0$.

As erosion progresses, the ridges will change shape and fill, thus η also will be a function of Q, which we need to determine. For a constant windspeed, horizontal flux (q) and wavelength (λ), the regression equation for η reduces to

$$\eta = -C_1 + C_4 A \qquad [8]$$

where C_1 and C_4 are constants and

$$A = A_0 - h - a \qquad [9]$$

Initial ridge height is A_0, while h and a represent height reductions by filling and soil loss from the ridge top area, respectively (figure 8).

We can approximate h as

$$h = [\lambda V_3/2]^{1/2} \qquad [10]$$

where V_3 is filled volume $[L^3/L^2]$. A regression equation fitted to exact calculations of a gives

$$a = d\,(V_2)^e \qquad [11]$$

where d and e are constants.

V_1 and V_2 are top loss volume with dimensions $[L^3/L^2]$, and a is zero until top loss exceeds V_1. Now

$$V_1 + V_2 = (E + \bar{C}aQ)/\rho_b \qquad [12]$$

and

$$V_3 = \bar{\eta}\, Q/\rho_b \qquad [13]$$

where ρ_b is soil bulk density, and $\bar{\eta}$ is defined as

$$\bar{\eta}(T,x) = \int^T \eta(t,x)q(t)dt \Big/ \int^T q(t)dt \qquad [14]$$

An equation for η as a function of Q is then

$$\eta = -C_1 + C_4 \left\{A_0 - (\bar{\eta}Q)^{1/2}\left[\frac{\lambda}{2\rho_b}\right]^{1/2} - d\left[\frac{E + \bar{C}aQ}{\rho_b} - V_1\right]^e\right\} \qquad [15]$$

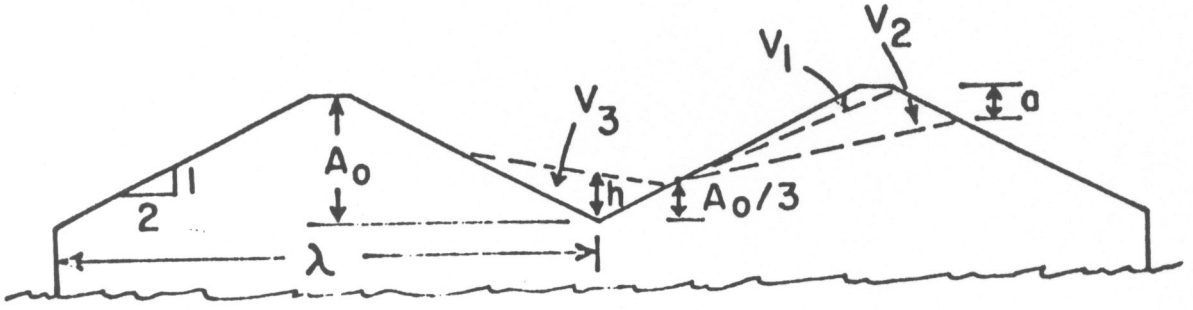

Figure 8 Ridge schematic with notation used in text.

Numerical solutions for η were calculated and found to fit approximately the expression

$$\eta = \eta_0 - g \ln Q, \ \eta > 0, \ Q \geq 1 \qquad [16]$$

where η_0 is initial ridge trapping efficiency at $A = A_0$, and g is a constant. Integrating the preceeding equation for $Q \geq 1$ to find $\bar{\eta}$ gives

$$\bar{\eta} = (\eta_0 + g) - (\eta_0 + g)/Q - g \ln Q \qquad [17]$$

and putting this approximation into equation 7 gives

$$\frac{dQ}{dx} = E + \bar{C} Q - [(\eta_0 + g) - (\eta_0 + g)/Q - g \ln Q] Q \qquad [18]$$

The preceeding equation was applied to an unridged surface and two ridged surfaces that have the shape shown in figure 8 with the dimensions and constants shown in Table 2. The E-value of 2.0 Kg/m² selected for the fields corresponds to a soil cloddiness (> 0.84 mm diameter) of about 10 percent for the ridged fields and slightly greater for the unridged field.

Plots of numerical solutions of Q - vs - X are shown in figure 9. The 10 cm ridges stabilized and dQ/dx approached zero at 30 to 40 m downwind while η remained at about 0.06 after erosion ceased. In contrast, on the 5 cm ridges dQ/dx did not approach zero, but instead η approached zero (the ridges failed) at Q equal 91.2 Kg/m at an X between 70 and 80 m downwind. Beyond that point, their effect on soil transport was similar to the unridged surface. Finally, the unridged surface ($\bar{\eta}$ equal zero) exhibited the exponential increase in soil flux passage one expects for the stated conditions.

From the example, it is clear that on both the unridged and 5 cm ridged fields the length of the eroding field must be controlled by some form of soil trap, such as a vegetative barrier, if adequate erosion control is to be maintained. Alternatively, one could increase surface cloddiness or vegetation on these fields to also provide control. The 10 cm ridges did not fail

Table 2. Values for unridged and ridged surfaces used in example calculations.

A_0 (cm)	λ (cm)	ρ_b (Kg/m^3)	E (Kg/m^2)	$\overline{Ca}$ (^{1}/m)	V_1 (m^3/m^2)	n_0 (^{1}/m)	d	e	C_1	C_4 (^{1}/m^2)	g
0	0	1400	2.0	.01	0.0	0.0					
5	21.5	1400	2.0	.01	.00115	.069	1.97	0.79	0.19	0.0519	0.0154
10	43.0	1400	2.0	.01	.00235	.115	2.28	0.81	0.19	0.0305	0.0168

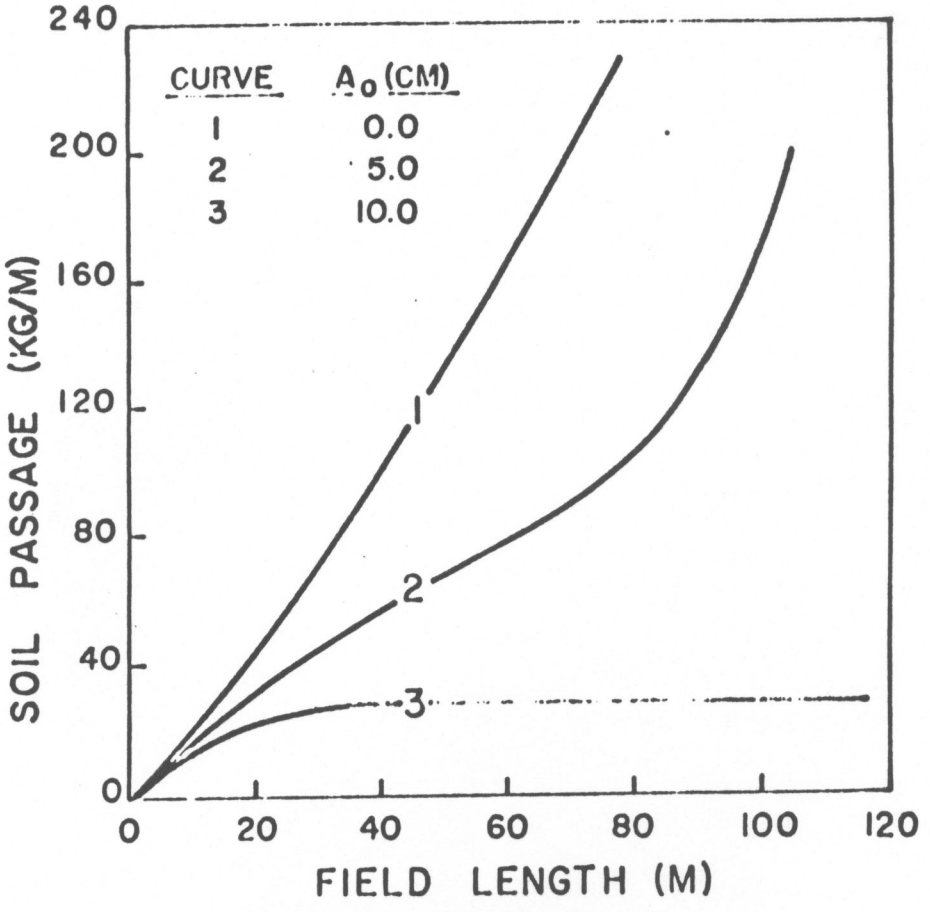

Figure 9 Effect of ridge amplitude on calculated soil loss at various distances downwind.

because they had a high initial n which prevented excessive abrasion of the downwind area and also the interridge volume necessary to hold all the soil that was removed from the ridge tops so control of field length was unnecessary.

References

Armbrust, D.V., Chepil, W.S., and Siddoway, F.H. (1964): Effects of ridges on erosion of soil by wind. Soil Sci. Soc. Amer. Proc. 28, 557-560.

Bagnold, R.A. (1941): The Physics of Blown Sands and Desert Dunes. Methuen, London. (Reprint 1973, published by Chapman and Hall, London.)

Chepil, W.S. and Woodruff, N.P. (1963): The physics of wind erosion and its control. Advances in Agronomy 15, 211-302.

Cole, G.W. (1984): A method for determining field wind erosion rates from wind-tunnel-derived functions. Trans. Amer. Soc. Agr. Engin. 27, 110-116.

Fryrear, D.W. (1984): Soil cover and wind erosion. Amer. Soc. Agr. Engin. Nat. Symp. on Erosion and Soil Productivity, Paper No. 84-ER01.

Gillette, D.A. (1977): Fine particulate emissions due to wind erosion. Trans. Amer. Soc. Agr. Engin. 20, 890-897.

Hagen, L.J. (1984): Soil aggregate abrasion by impacting sand and soil particles. Trans. Amer. Soc. Agr. Engin. 27, 805-808, 816.

Hagen, L.J. and Lyles, L. (1985): Amount and nutrient content of particles produced by soil aggregate abrasion. Erosion and Productivity, Amer. Soc. Agr. Engin. ASAE Publication 8-85, 117-129.